2009 American Control Conference
Hyatt Regency Riverfront, St. Louis, MO, USA
June 10-12, 2009

Robust Fixed-Structure Controller Design of Electric Power Steering Systems

Ahmed H. El-Shaer, Sumio Sugita and Masayoshi Tomizuka

***Abstract*— This paper presents a two-degree-of-freedom controller structure for electric power steering systems. The controller is synthesized using a hybrid linear matrix inequality and genetic algorithms optimization. Robust stability is studied for both sector-bounded and passive uncertainties resulting in a system of linear matrix inequalities (LMIs) and a linear matrix equality (LME). This system of LMIs/LME defines a guaranteed cost H_2 optimization subject to an $\mathrm{H}_\infty-$norm performance as well as a strict-positive-real constraints. Experimental results involving human-in-the-loop show that the control design did satisfy the criteria for robust control and performance. Furthermore, the ease-of-tuning of the proposed controller structure makes it possible to improve the steering "feel".**

I. INTRODUCTION

In recent years, there has been noticeably increasing interest within the automotive industry in electric power steering (EPS) systems technology as a viable replacement of the more conventional hydraulic power steering. This transition is justified on the grounds of four main points [6, 9]: (1) ease of tunability: EPS systems are examples of mechatronic systems which employ programmable features making them easily adjustable to wider ranges of operation, (2) fuel economy: Electric-motor-powered EPS systems are on-demand systems that operate only when the steering wheel is turned, (3) modularity: EPS systems are inherently modular since they are composed of more compact components that are easily packaged into separate subsystems, (4) environmental friendliness: EPS systems remove the need for hydraulic oil refills as well as oil leakage problems. The second item above is an attractive advantage of EPS systems since they can offer lower energy consumption than conventional hydraulic power steering systems. It has been reported in [3] that among the different types of power steering systems available for passenger vehicles, EPS systems offer the lowest power consumption. In particular, EPS systems achieve power consumption savings in excess of 50% of the consumption of other power steering systems such as hydraulic power steering and electro-hydraulic power steering systems [3].

In contrast to many conventional feedback systems such as motion control applications, EPS systems do not have well defined feedback design measures such as tracking error signals. On the other hand, performance criteria such as "comfort" and "feel" are subjective since they vary among drivers and according to driving conditions. Furthermore, they are difficult to quantify using available physical measurements. In addition, the presence of the human-in-the-loop make control design tasks of EPS systems very challenging. This paper presents a two-degree-of-freedom (2-DOF) fixed-structure controller design for the EPS system which satisfies closed loop passivity constraint. The paper addresses the robust stability of the feedback interaction between the driver, the EPS system and the vehicle force impedance. The controller-design problem is formulated using a system of linear matrix inequalities (LMIs)/linear matrix equality (LME), which describe performance objectives as well as the passivity constraint given by the positive real lemma. Hardware-in-the-loop (HIL) experiments are conducted to investigate the steering "feel" performance of the synthesized 2-DOF controller structure.

The control of EPS systems has been reported by a vast number of researchers [5, 6, 16]. In [16], Zaremba et. al. studied performance requirements such as torque amplification and suppression of oscillations resulting from the lightly damped mode due to the torsion bar. The control synthesis presented in this work is based on the closed loop H_2-norm minimization utilizing fixed structure phase compensators. In [6], Rakan et. al. employed the H_∞ optimization framework to achieve assist torque generation, driver's appropriate road-feel and closed loop robustness. The controller structure proposed has a feed-forward component and a feedback component which is synthesized using $\mathrm{H}_\infty-$weighted sensitivity minimization. In [5], Canudas-De-Wit et. al. approached the EPS control design using a passivity-based impedance-shaping controller. In this study, the authors addressed the lack of quantifiable control-design metrics by choosing the technique of impedance shaping which employs a master-slave loop structure. The impedance chosen defines desired dynamics from the driver input torque to the steering wheel angular position.

This paper is organized as follows, Section 2 presents mathematical models of a column-assist EPS system and road-tire force impedance and discusses the interaction between them. In Section 3, control design objectives and the 2-DOF controller structure are given. Section 4, presents robust stability analysis of the EPS closed loop system. In Section 5, the 2-DOF controller is synthesized using a hybrid LMI/genetic algorithm (GA) optimization method. In section 6, simulation and experimental results are presented.

II. EPS/VEHICLE MODELING AND INTERACTION

The work presented in this paper focuses on column-assist EPS systems. However, the analysis carried out can be easily extended to the other types of EPS systems, steer-by-wire systems [1], and more generally to other applications involving human-in-the-loop interaction. In [9], a 4^{th} order model in state space form for the column-assist EPS system (Fig. 1) is developed and validated.

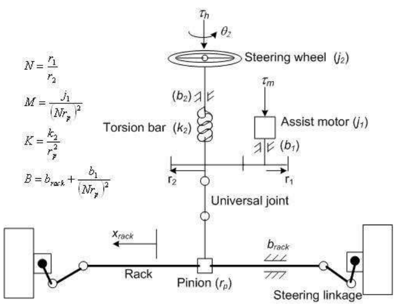

Fig. 1. Schematic diagram of column-assist EPS

Ahmed H. El-Shaer is with the Department of Mechanical Engineering, University of California at Berkeley, Berkeley, CA 94720 (ashaer@newton.berkeley.edu)

Sumio Sugita is with NSK research and development center, Japan. Now is visiting industrial fellow at the Mechanical Engineering, University of California, Berkeley, CA 94720 (sugitas@me.berkeley.edu)

Masayohsi Tomizuka is with the Department of Mechanical Engineering, University of California at Berkeley, Berkeley, CA 94720 (tomizuka@me.berkeley.edu)

The linearized state space model representation of this column-assist EPS is given by

$$\begin{aligned}\dot{\mathrm{x}} &= \begin{bmatrix} 0 & 1 & 0 & 0 \\ -\frac{k_2}{j_2} & -\frac{b_2}{j_2} & \frac{k_2}{r_p j_2} & 0 \\ 0 & 0 & 0 & 1 \\ \frac{k_2}{r_p M} & 0 & -\frac{K}{M} & -\frac{B}{M} \end{bmatrix} \mathrm{x} \\ &+ \begin{bmatrix} 0 & 0 & 0 \\ \frac{1}{j_2} & 0 & 0 \\ 0 & 0 & 0 \\ 0 & \frac{1}{M} & -\frac{1}{M} \end{bmatrix} \begin{bmatrix} \tau_h \\ f_{dist} \\ f_{SAM} \end{bmatrix} + \begin{bmatrix} 0 \\ 0 \\ 0 \\ \frac{1}{N r_p M} \end{bmatrix} \tau_m \\ \mathrm{y} &= \begin{bmatrix} k_2 & 0 & -\frac{k_2}{r_p} & 0 \\ 0 & 0 & 1 & 0 \end{bmatrix} \mathrm{x} \qquad (1)\end{aligned}$$

where the state vector is defined by: $\mathrm{x} = \begin{bmatrix} \theta_2 & \dot{\theta}_2 & x_{rack} & \dot{x}_{rack} \end{bmatrix}^{\mathrm{T}}$ (see Fig. 1 for variable definitions). The input disturbance vector is comprised of the driver torque (τ_h), the road-tire disturbance forces (f_{dist}) and the force due to the self-aligning moment (f_{SAM}). The control input consists of the motor input torque (τ_m). Moreover, the first component of the output vector y is the torsion bar torque (τ_b), and the second component is the rack displacement (x_{rack}). Assuming that the vehicle forward velocity is held constant and the road-tire steering angle is small, the force impedance for the self-aligning moment (SAM) is given by the following 2^{nd} order transfer function [9]:

$$G_{x_{rack} \to f_{SAM}}(\mathrm{s}) = \frac{2tC_1}{l^2} \frac{\mathrm{s}^2 + d_1 \mathrm{s} + d_0}{\mathrm{s}^2 + b_1 \mathrm{s} + b_0} \qquad (2)$$

where l is the length of the steering knuckle-arm, C_1 is the front tires's cornering stiffness and t is the dynamic caster moment arm. The transfer function coefficients are given by $d_1 = 2\frac{C_2\left(I_z + l_2^2 m_{tot}\right)}{m_{tot} I_z v_x}$, $d_0 = 2\frac{C_2 l_2}{I_z}$, $b_1 = 2\frac{I_z(C_1+C_2)+\left(C_1 l_1^2 + C_2 l_2^2\right)}{m_{tot} I_z v_x}$ and $b_0 = \frac{2}{I_z}\left(-C_1 l_1 + C_2 l_2 + 2\frac{C_1 C_2 (l_1+l_2)^2}{m_{tot} v_x^2}\right)$.

A. Passivity of the Road-Tire Force Impedance

Assuming that the stability conditions are satisfied in Eq. 2 (i.e. $b_1 > 0$ and $b_0 > 0$), the transfer function $G_{\dot{\delta} \to f_{SAM}}(\mathrm{s}) := \frac{G_{\delta \to f_{SAM}}(\mathrm{s})}{\mathrm{s}}$ is passive if and only if it is positive real (PR) [10]. This is satisfied if and only if $\mathrm{Re}\left\{\mathrm{G}_{\dot{\delta} \to f_{SAM}}(j\omega)\right\} \geq 0$ for all $\omega \in \mathbb{R}$. Carrying out the required computations and simplifying terms, the transfer function $G_{\dot{\delta} \to f_{SAM}}(\mathrm{s})$ is positive real if and only if [9]:

$$2C_2 (l_1 + l_2)\left(I_z + l_2^2 m_{tot}\right) - m_{tot}(I_z + l_1 l_2) v_x^2 > 0 \qquad (3)$$

The condition given by Eq. 3 is plotted in Fig. 2. This figure shows that unlike passive environments commonly encountered in tele-manipulated robots [7], the road-tires' self-aligning moments exhibit non-passive behavior over a large range of v_x and μ. Hence, this shortage of passivity has to be accounted for, to realistically address the uncertainty involved in the EPS environment [1].

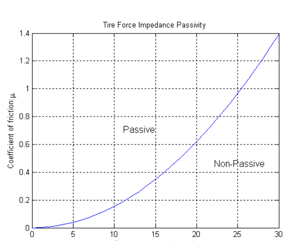

Fig. 2. Tire force impedance passivity

B. Open loop behavior

The block diagram given in Fig. 3 shows the assist-torque open loop for a given vehicle forward velocity v_x. In this diagram, the transfer functions $G_1(\mathrm{s})$ and $G_2(\mathrm{s})$ represent the open loop transfer functions from τ_h and τ_m to the torsion bar torque τ_b, respectively. Moreover, the boost gain nonlinearity (Fig. 3) $\phi(.,.)$: $\mathbb{R} \times \mathbb{R}_+ \to \mathbb{R}$ belongs to the sector given by $\left[0,\ \bar{\mathrm{k}}_\phi\right]$. This nonlinearity is "tuned" to set the appropriate desired current $\mathrm{I_{Des}}$ for the assist-torque motor at a given velocity v_x [9]. Thus, in the following sections, the boost gain will be a given nonlinearity as shown in Fig. 3. It is noted that the boost gain function is deliberately designed to have "dead-zone" behavior near the origin to reduce the sensitivity of the EPS actuator.

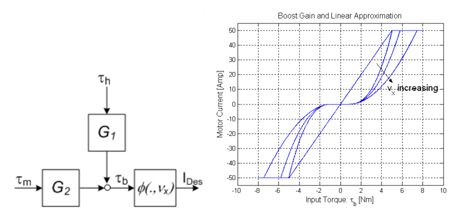

Fig. 3. Open loop block diagram (left), boost gain nonlinearity $\phi(., v_x)$ (right)

To show the effect of this nonlinearity on the closed loop system, the Bode plot of $G_2(\mathrm{s})$ is drawn for a different values of v_x while setting the boost-gain nonlinearity to the maximum value of the sector bound; that is $\phi(\tau_b(\mathrm{t}), v_x(\mathrm{t})) = 10\tau_b$ (Fig. 3). This worst-case analysis shows that the open loop system for large values of the boost gain has a very low phase margin which implies that the closed loop system lacks robustness.

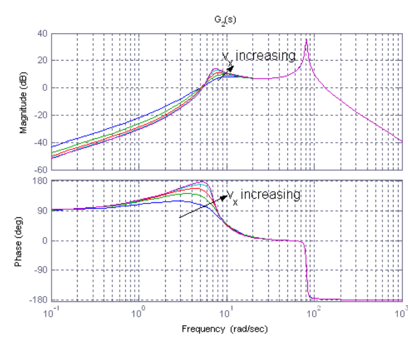

Fig. 4. Bode plot of $G_2(\mathrm{s})$

C. Role of Passivity

Electric power steering systems are examples of driver-assisting devices that are physically driven by a human operator. This direct man-machine interaction places stringent requirements on the feedback design for EPS systems to insure safe operation by the human operator. Passivity has long been the framework to study robust stability and performance for applications involving human interaction such as tele-manipulated robot arms [7, 11]. In particular, passive dynamical systems are systems which do not generate energy, but either store or dissipate energy. Consequently, passive systems behave "friendly" in the environments where they operate [11]. Specifically, the human arm impedance is bilaterally coupled to the EPS system via the human input torque (τ_h) and the steering wheel angular velocity $\left(\omega = \dot{\theta}_2\right)$ as shown in Fig. 5. Thus the passivity of the EPS feedback system ensures that the energy resulting from the human input torque satisfies [8, 10]:

$$-\int_0^T \tau_h \dot{\theta}_2 dt < \infty, \quad \forall T > 0 \tag{4}$$

The condition given in Eq. 4 implies that the feedback system in Fig. 5 is stable since only a finite amount of energy could be extracted while the system is excited by τ_h. Moreover, passivity guarantees closed loop robust stability for all passive un-modeled dynamics between the port variables τ_h and $\dot{\theta}_2$. In Fig. 5, the driver's arm impedance is modeled by passive (possibly nonlinear dynamics). In [14], it was found that a single-degree-of-freedom model made of linear mass-spring-damper fitted experimental data well under normal operating conditions (i.e. absence of drugs or alcohol). In other studies [1], the spring-mass-damper is used to model the human arm impedance. This model is given by:

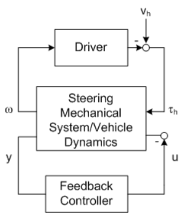

Fig. 5. Closed loop feedback block diagram, v_h is the neural muscle command

$$Z_d(s) \triangleq \frac{\tau_h(s)}{\omega(s)} = D_d + \frac{C_d}{s} + J_d s \tag{5}$$

where τ_h is the torque, ω is the steering wheel angular velocity, D_d is the viscous damping, C_d is the stiffness, J_d is the inertia term. However, it is clear that the model parameters in Eq. 5, are case-dependent. Hence, robust stability is ensured by enforcing closed loop passivity of the map $\tau_h \to \omega$ which guarantees that the negative feedback interconnection of the human arm impedance and the EPS actuator is asymptotically stable [10].

III. Control Design Objectives and Controller Structure

Despite difficulties encountered in quantifying performance criteria for EPS feedback systems, the following two points address the general desired performance [9]:

1) Driver feel: appropriate driver steering "feel" is achieved by tracking the boost gain (i.e. assist-torque) without introducing large delays in the feedback system resulting from the narrow bandwidth control design. Furthermore, the controller needs to attenuate the effects of road-tire disturbance forces originating from road surface irregularities, tire imbalance or any other disturbance source,
2) Closed loop robustness: closed loop stability must be maintained in the presence of the boost-gain nonlinearity (Fig. 3) and model parameter uncertainties. In addition, the human driver introduces an additional loop to the feedback system generated by the muscle impedance actuation as depicted in Fig. 5.

For the sake of control synthesis and analysis of closed loop robust stability, the negative feedback interconnection of EPS/vehicle dynamics (Eqs. 1 and 2) is be represented by the following 6^{th} order model:

$$\begin{aligned}
\dot{x} &= Ax + B_1 w_1 + B_2 w_2 + B_u u \\
z_1 &= C_1 x \\
z_2 &= C_2 x + D_2 u \\
z_\infty &= C_3 x + D_4 u \\
y &= C_4 x + \nu \\
w_1 &= -\Delta(z_1)
\end{aligned} \tag{6}$$

where $x(t)$ is the state vector, $w_1(t)$ is the driver input torque, $w_2(t)$ is the road disturbance forces, $u(t)$ is the assist-motor torque control input, $z_1(t)$ is the steering wheel angular velocity and $\Delta(.)$ is the passive muscle impedance dynamics. The vectors $z_2(t)$ and $z_\infty(t)$ define performance output vectors associated with the closed loop H_2 and H_∞ performance criteria, respectively (defined below), and $y(t)$ is the output vector composed of the torque sensor and rack displacement (Eq. 1) corrupted by measurement noise $\nu(t)$.

A. Controller Structure

From the previous discussion, it is clear that phase compensation is required to enhance the robustness of the EPS feedback system against parameter variations. Moreover, the torsion bar mode needs to be damped by employing velocity feedback. Consequently, a 2-DOF controller will be considered for the EPS closed loop system. The first component of this controller is the phase compensator, denoted by $G_{c1}(s)$, while the second component is comprised of a state feedback controller employing the rack displacement and velocity, denoted as $G_{c2}(s)$. Hence if $G_{c2}(s)$ is an SPR transfer function, in addition to the phase compensation provided by $G_{c1}(s)$, the feedback of the steering subsystem and the rack/vehicle subsystem can be rendered passive making the closed loop map: $\tau_h \to \dot{\theta}_2$ strictly passive. Thus, the 2-DOF compensator to be designed is given by:

$$u(s) = -G_{c2}(s)\dot{x}_{rack}(s) + G_{c1}(s)\eta(s) \tag{7}$$

where $\eta(t) = \phi(\tau_b(t), v_x(t))$, and the compensator transfer function $G_{c2}(s)$ is given by:

$$G_{c2}(s) = B_{c2} + \frac{K_{c2}}{s} \tag{8}$$

Two possible network cascades will be chosen for the phase compensator $G_{c1}(s)$ [9, 16]:

1) Triple lead with a lag filter:

$$G_{c1}(s) = \frac{p_{lag}}{s + p_{lag}} \prod_{i=1}^{3} \frac{1}{\beta_i} \frac{s + z_i}{s + p_i} \quad \beta_i \triangleq \frac{z_i}{p_i} \; i = 1 \cdots 3 \tag{9}$$

2) Lag with a notch filter:

$$G_{c1}(s) = \frac{p_{lag}}{s + p_{lag}} \left(\frac{p_1 p_2}{\omega_0^2}\right) \frac{s^2 + 2\xi\omega_0 s + \omega_0^2}{(s + p_1)(s + p_2)} \tag{10}$$

where $\beta_i \; i = 1 \cdots 3$ is the lead ratio and ω_0 will be set to 12 Hz. It is obvious that each $G_{c1}(s)$ as defined will have a DC gain equal 1. Thus, the boost gain does not get amplified or attenuated in the feedback loop. Moreover, from the control objectives defined above, it is desired that the phase $\phi(j\omega)$ for each compensator $G_{c1}(s)$ satisfies $-20^\circ \le \phi(j\omega) \le 50^\circ \;\; \forall \omega > 0$ [9, 16].

B. Performance Measures

The driver feel and stability robustness are two important control design objectives for EPS systems. In order to satisfy the driver feel objective, the following performance measure is defined:

$$J_1 = \|T_{w_1 \to z_2}\|_2 \tag{11}$$

where $T_{w_1 \rightarrow z_2}$ denotes the closed loop map from the input torque disturbance w_1 to the performance output z_2 and $\|.\|_2$ is the standard H_2 norm. The performance output z_2 in Eq. 11 is given by the following equation:

$$z_2 = \begin{bmatrix} 0 & q_1 & 0 & 0 & 0 & 0 \\ 0 & 0 & 0 & q_2 & 0 & 0 \\ 0 & 0 & 0 & 0 & 0 & 0 \end{bmatrix} x + \begin{bmatrix} 0 \\ 0 \\ \rho_1 \end{bmatrix} u \qquad (12)$$

where the weighting parameters q_1, q_2 and ρ_1 are all positive constants. With this definition, the performance objective in Eq. 12 represents the standard LQR cost function $\int_0^\infty \left(q_1 \dot{\theta}_2^2 + q_2 \dot{x}_{rack}^2 + \rho_1 u^2 \right) dt$ which is a weighted sum of the system states related to the kinetic energy of the EPS system and the control input. To account for the effect of road-tire disturbance forces acting on the rack, the following performance measure is considered:

$$J_2 = \|T_{w_2 \rightarrow z_\infty}\|_\infty \qquad (13)$$

where $T_{w_2 \rightarrow z_\infty}$ denotes the closed loop sensitivity function from the input road-tire disturbance to the performance output z_∞ and $\|.\|_\infty$ is the H_∞ norm. The performance output z_∞ is taken to be:

$$z_\infty = q_3 \begin{bmatrix} k_2 & 0 & -\frac{k_2}{r_p} & 0 & 0 & 0 \\ 0 & 0 & 0 & 0 & 0 & 0 \end{bmatrix} x + \begin{bmatrix} 0 \\ \rho_2 \end{bmatrix} u \qquad (14)$$

Similarly, the weighting design parameters q_3 and ρ_2 are positive constants. It is clear that z_∞ considers the effect of the road-tire disturbances on the torsion bar signal and the control input. The reason for choosing the torsion bar signal is the central role it plays in EPS feedback system functionality by setting the appropriate assist-torque.

IV. Robust Stability Analysis

Stability analysis is fundamentally important for robust control design of EPS feedback systems. The uncertain system given in Eq. 6 involves the passive driver muscle impedance $\Delta(.)$ and the sector-bounded boost gain nonlinearity $\phi(\tau_b(t), v(t))$ employed by the controller. Consequently, Eq. 6 can be represented using a linear fractional transformation (LFT) block diagram (Fig. 6). Furthermore, a loop transformation is introduced around the boost gain nonlinearity where $c_\phi = \frac{\bar{k}_\phi}{2}$. In addition to reducing conser-

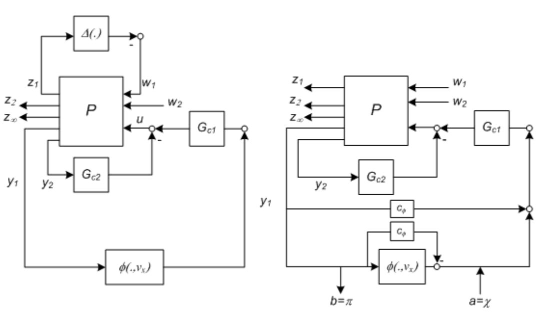

Fig. 6. LFT for robust stability (left), Loop transformation (right)

vatism, it is well known that the loop transformation introduced in Fig. 6 does not change the feedback loops and induces the norm-bound $\|\chi\| \leq r_\phi \|\pi\|$ where $r_\phi = \frac{\bar{k}_\phi}{2}$ [8]. Hence, given a feedback compensator (Eq. 7) which internally stabilizes the closed loop EPS/vehicle system, robust stability and performance are analyzed, in the presence of $\Delta(.)$ and the sector bounded nonlinearity $\phi(.,.) \in [0, \bar{k}_\phi]$, by considering the following two problems:

1) Robust strict positive realness:
The closed loop EPS system (Eqs. 6, 7) is robustly stable if the closed loop map $w_1 \rightarrow z_1$ is strictly positive real (SPR),
2) Robust disturbance attenuation:
The closed loop map $T_{w_2 \rightarrow z_\infty}$ satisfies $\|T_{w_2 \rightarrow z_\infty}\|_\infty \leq \gamma$ for a given $\gamma > 0$.

After standard algebraic manipulations of Eqs. 6, 7 and 8, the closed loop system with the loop transformation is given by the following state space representation:

$$\begin{aligned} \dot{\tilde{x}} &= \left(\tilde{A} + \frac{\bar{k}_\phi}{2} \tilde{B}_u \tilde{C}_4 \right) \tilde{x} + \tilde{B}_1 w_1 + \tilde{B}_2 w_2 + \tilde{B}_u \chi \\ z_1 &= \tilde{C}_1 \tilde{x} \\ z_2 &= \tilde{C}_2 \tilde{x} \\ z_\infty &= \tilde{C}_3 \tilde{x} \\ w_1 &= -\Delta(z_1) \end{aligned} \qquad (15)$$

A. Robust Strict Positive Realness

The following theorem gives a sufficient condition for robust stability of the uncertain system given in Eq. 6. Applying the S-procedure [4], the following result, with $w_2 = 0$ is obtained.

Theorem 1: Given the internally stabilizing feedback compensator in Eq. 7, the uncertain system in Eq. 6 is globally asymptotically stable for all passive systems (possibly nonlinear) $\Delta(.)$ and sector bounded nonlinearities $\phi(.,.)$ which belong to the sector $[0, \bar{k}_\phi]$, if for the following closed loop system

$$\begin{aligned} \dot{\tilde{x}} &= \left(\tilde{A} + \frac{\bar{k}_\phi}{2} \tilde{B}_u \tilde{C}_4 \right) \tilde{x} + \tilde{B}_1 w_1 + \tilde{B}_u \chi \\ z_1 &= \tilde{C}_1 \tilde{x} \\ w_1 &= -\Delta(z_1) \end{aligned} \qquad (16)$$

there exist a positive definite symmetric matrix $Y \succ 0$ and a scaling multiplier $\tau_1 \geq 0$ such that

$$2\tilde{x}^T Y \left(\bar{A}\tilde{x} + \tilde{B}_u \chi \right) + \tau_1 \left(r_\phi^2 \tilde{x}^T \tilde{C}_4^T \tilde{C}_4 \tilde{x} - \chi^T \chi \right) < 0 \qquad (17)$$

$$Y\tilde{B}_1 = \tilde{C}_1^T \qquad (18)$$

where $\bar{A} = \left(\tilde{A} + \frac{\bar{k}_\phi}{2} \tilde{B}_u \tilde{C}_4 \right)$.

Proof: Differentiating the positive definite function $V(\tilde{x}) = \tilde{x}^T Y \tilde{x}$ along an arbitrary trajectory of the system in Eq. 16, it is clear that the conditions given in Eqs. 17 and 18 imply that $\dot{V}(\tilde{x}) - 2z_1^T w_1 < 0$. Thus, the map $w_1 \rightarrow z_1$ is strictly passive with respect to the positive definite storage function $\frac{V(\tilde{x})}{2}$. Asymptotic stability of Eq. 15 follows from that of the negative feedback interconnection of passive systems [10] ■.

It is noted that in the case when the nonlinearity $\phi(.,.)$ is replaced by a linear gain, global asymptotic stability is established if the feedback system is SPR [2].

B. Robust Disturbance Attenuation

Having established asymptotic stability of the negative feedback interconnection in Eq. 15, disturbance attenuation due to w_2 is considered independently of w_1. This is done by enforcing an upper bound γ on the H_∞ norm of the objective given in Eq. 13 such that $\|T_{w_2 \rightarrow z_\infty}\|_\infty \leq \gamma$. Applying the S-procedure, the following result directly follows [4].

Theorem 2: Given the internally stabilizing feedback compensator in eq. 7, if there exist a positive definite symmetric matrix $X \succ 0$

and a scaling multiplier $\tau_2 \geq 0$ such that

$$2\tilde{\mathrm{x}}^{\mathrm{T}}\mathrm{X}\left(\bar{\mathrm{A}}\tilde{\mathrm{x}}+\tilde{\mathrm{B}}_2 w_2+\tilde{\mathrm{B}}_u\chi\right)+\tau_2\left(\mathrm{r}_\phi^2\tilde{\mathrm{x}}^{\mathrm{T}}\tilde{\mathrm{C}}_4^{\mathrm{T}}\tilde{\mathrm{C}}_4\tilde{\mathrm{x}}-\chi^{\mathrm{T}}\chi\right) \\ -\gamma^2 w_2^T w_2+\tilde{\mathrm{x}}^{\mathrm{T}}\tilde{\mathrm{C}}_3^{\mathrm{T}}\tilde{\mathrm{C}}_3\tilde{\mathrm{x}} \leq 0 \quad (19)$$

then the closed loop system in Eq. 15 with $w_1 = 0$, is asymptotically stable and $\|T_{w_2\rightarrow z_\infty}\|_\infty \leq \gamma$.

V. Fixed Structure Optimal Control Synthesis

A. Guaranteed Cost Formulation

The controller synthesis is formulated as a guaranteed cost optimization problem. The following corollary extends the robust stability analysis given in Theorem 1 to a robust H_2 optimization problem.

Corollary 1: Suppose that the conditions in Theorem 1 are satisfied with Eq. 17 changed to

$$2\tilde{\mathrm{x}}^{\mathrm{T}}\mathrm{Y}\left(\bar{\mathrm{A}}\tilde{\mathrm{x}}+\tilde{\mathrm{B}}_u\chi\right)+\tau_1\left(\mathrm{r}_\phi^2\tilde{\mathrm{x}}^{\mathrm{T}}\tilde{\mathrm{C}}_4^{\mathrm{T}}\tilde{\mathrm{C}}_4\tilde{\mathrm{x}}-\chi^{\mathrm{T}}\chi\right)+ \\ \tilde{\mathrm{x}}^{\mathrm{T}}\mathrm{Q}\tilde{\mathrm{x}}<0 \quad (20)$$

for some positive semidefinite symmetric matrix $\mathrm{Q} \succeq 0$. Then there exists a constant c such that

$$\int_0^\infty \tilde{\mathrm{x}}^{\mathrm{T}}\mathrm{Q}\tilde{\mathrm{x}}dt < \tilde{\mathrm{x}}^{\mathrm{T}}(0)\,\mathrm{Y}\tilde{\mathrm{x}}(0)+2c^2 \quad (21)$$

Proof: This result follows from using the conditions in Theorem 1 and noting that Eq. 20 provides an upper bound for Eq. 17, which implies that the system in Eq. 16 is asymptotically stable. Integrating the left hand side of Eq. 20 along an arbitrary trajectory of the system in Eq. 16, the following is obtained:

$$\tilde{\mathrm{x}}^{\mathrm{T}}(T)\,\mathrm{Y}\tilde{\mathrm{x}}(T)-\tilde{\mathrm{x}}^{\mathrm{T}}(0)\,\mathrm{Y}\tilde{\mathrm{x}}(0)+2\int_0^T z_1^{\mathrm{T}}(-w_1)\,dt < -\int_0^T \tilde{\mathrm{x}}^{\mathrm{T}}\mathrm{Q}\tilde{\mathrm{x}}dt \quad (22)$$

From the passivity of $\Delta(.)$, it follows that $\int_0^\infty z_1^{\mathrm{T}}(-w_1)\,dt \geq -c^2$ for some constant c [8]. Thus, letting $T \rightarrow \infty$ and rearranging terms, Eq. 21 is arrived at ■.

In particular, if the matrix Q is written as $\mathrm{Q}=\tilde{\mathrm{C}}_2^{\mathrm{T}}\tilde{\mathrm{C}}_2$, it follows that for the feedback system in Eq. 16, the H_2 norm of the output defined by $z_2 \triangleq \tilde{\mathrm{C}}_2\tilde{\mathbf{x}}$ is upper bounded by $\tilde{\mathbf{x}}(0)^{\mathrm{T}}\,\mathrm{Y}\tilde{\mathbf{x}}(0)$ where Y satisfies Eqs. 17 and 18. Moreover, in the case of linear $\Delta(.)$ (Eq. 5), c in Eq. 21 can be set equal to zero [8].

B. Controller Synthesis

In the following presentation, unknown controller parameters (Eqs. 8, 9 and 10) are expressed as a row vector $\Theta \in \mathbb{R}^{1\times\mathrm{N}}$ where N is the number of unknown parameters. Consequently, the closed loop system can be expressed as a function of the unknown parameters Θ (i.e. $\bar{\mathrm{A}}(\Theta)$, etc.). With this notational convenience the guaranteed-cost optimal control problem for the closed loop system is defined, given $\Theta\ \left(\in \mathbb{R}^{1\times\mathrm{N}}\right), \tilde{\mathrm{x}}(0)\ (\in \mathbb{R}^{\mathrm{n}})$ and $\gamma_{max}\ (\in \mathbb{R})$ such that $\gamma \leq \gamma_{max}$, by the following system of LMIs/LME:

$$\min_{\mathrm{Y},\mathrm{X},\kappa,\tau_1,\tau_2} \quad \mathrm{trace}\left(\tilde{\mathrm{x}}(0)^{\mathrm{T}}\,\mathrm{Y}\tilde{\mathrm{x}}(0)\right)$$
$$\text{subject to}:$$
$$\mathrm{X}\succ 0,\ \mathrm{Y}\succ 0,\ \kappa>0,\ \sqrt{\gamma_{max}}\geq\gamma>0, \tau_1\geq 0,\ \tau_2\geq 0$$
$$\begin{bmatrix} \bar{\mathrm{A}}^{\mathrm{T}}\mathrm{Y}+\mathrm{Y}\bar{\mathrm{A}}+\tau_1\mathrm{r}_\phi^2\tilde{\mathrm{C}}_4^{\mathrm{T}}\tilde{\mathrm{C}}_4+\tilde{\mathrm{C}}_2^{\mathrm{T}}\tilde{\mathrm{C}}_2 & \mathrm{Y}\tilde{\mathrm{B}}_u \\ \tilde{\mathrm{B}}_u^{\mathrm{T}}\mathrm{Y} & -\tau_1\mathrm{I} \end{bmatrix} \prec 0 \quad (23)$$
$$\tilde{\mathrm{B}}_1^{\mathrm{T}}\mathrm{Y}=\kappa\tilde{\mathrm{C}}_1$$
$$\begin{bmatrix} \bar{\mathrm{A}}^{\mathrm{T}}\mathrm{X}+\mathrm{X}\bar{\mathrm{A}}+\tau_2\mathrm{r}_\phi^2\tilde{\mathrm{C}}_4^{\mathrm{T}}\tilde{\mathrm{C}}_4+\tilde{\mathrm{C}}_3^{\mathrm{T}}\tilde{\mathrm{C}}_3 & \mathrm{X}\tilde{\mathrm{B}}_u & \mathrm{X}\tilde{\mathrm{B}}_2 \\ \tilde{\mathrm{B}}_u^{\mathrm{T}}\mathrm{X} & -\tau_2\mathrm{I} & 0 \\ \tilde{\mathrm{B}}_2^{\mathrm{T}}\mathrm{X} & 0 & -\gamma\mathrm{I} \end{bmatrix} \preceq 0$$

The optimization problem given in Eq. 23 involves product terms between the controller and the optimization variables giving rise to bilinear matrix inequalities (BMIs). Optimization problems involving BMIs constraints are non-convex, NP hard problems [4]. However, given a candidate controller parameter vector Θ, the optimization problem in Eq. 23 is convex and hence can be solved efficiently using semidefinite programming (SDP). This motivates the use of global optimization techniques such as genetic algorithms (GA) [13] to search the controller parameter space. Once an optimal controller parameter vector Θ is produced by the GA code, the SDP in Eq. 23 can be solved using readily available software [12]. Recently, hybrid GA optimization techniques have gained attention as important tools to solve difficult optimization problems arising in control and/or estimation (see [9, 15]). The hybrid GA/LMI optimization algorithm described previously is depicted in the flow chart given in Fig. 7. In Fig. 7, Npop is the population size of

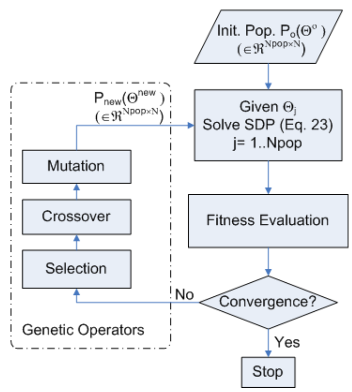

Fig. 7. Structure of hybrid GA\LMI

unknown controller parameters, $\mathrm{P}_{\mathrm{o}}(\Theta^o)$ is the initial population of randomly chosen controller parameters and $\mathrm{P}_{\mathrm{new}}(\Theta^{\mathrm{new}})$ is a new population produced by the GA operations (i.e. selection, crossover and mutation). The GA used in this paper has the following specifications [9]: (1) floating point representation, (2) tournament selection with linear ranking [13], (3) arithmetic cross-over, (4) uniform mutation, (5) elitism is applied. In particular, the closed loop matrix $\bar{\mathrm{A}}(\Theta) := \left(\bar{\mathrm{A}}+\frac{\bar{\mathrm{k}}_\phi}{2}\tilde{\mathrm{B}}_u\tilde{\mathrm{C}}_4\right)$ must be Hurwitz (i.e. $\mathrm{Re}\left\{\lambda_i\left(\bar{\mathrm{A}}(\Theta)\right)\right\} < 0 \ \ i=1,..,n$), since otherwise the LMI's in Eq. 23 will be infeasible. This condition constrains the choice of the controller-parameters search space since only internally stabilizing controllers are permissible. Consequently, for a given internally stabilizing controller parameter vector Θ, the associated optimization cost is given by:

$$cost\,(\Theta_j)=\begin{cases} \mathrm{trace}\left(\tilde{\mathrm{x}}(0)^{\mathrm{T}}\,\mathrm{Y}\tilde{\mathrm{x}}(0)\right) & \text{if Eq. 23 is satisfied} \\ \Gamma & \text{otherwise} \end{cases} \quad (24)$$

where $j=1,..,\mathrm{Npop}$ and Γ is a large penalty (e.g. 10^6) to lower the rank of these controllers in subsequent iterations.

C. Optimization and Simulation Results

The weighting parameters used in the performance measures (Eqs. 12 and 14) are $q_1 = 4, q_2 = 0.5, \rho_1 = 0.01$ and $q_3 = 5, \rho_2 = 0.01$. The upper bound γ_{max} is set equal to 0.5. Moreover, the vehicle velocity v_x and the road-surface friction coefficient μ are set equal to 30 m/sec and 0.6, respectively (i.e. extremely non-passive conditions). The GA parameters are set to $\mathrm{Npop}=50$, crossover probability equal to 0.6, mutation probability equal to 0.85 and the maximum number of generations used is 80. The minimum value achieved for the H_2-performance cost is equal to 8 for the closed loop system with the triple lead/lag compensator (Eqs. 8, 9). The Bode plots of the phase compensators (Eqs. 9 and 10) along with the compensated open loop transfer function $G_2(s)$ are given in Fig. 8 ($v_x = 30\ m/sec,\ \mu = 0.6$).

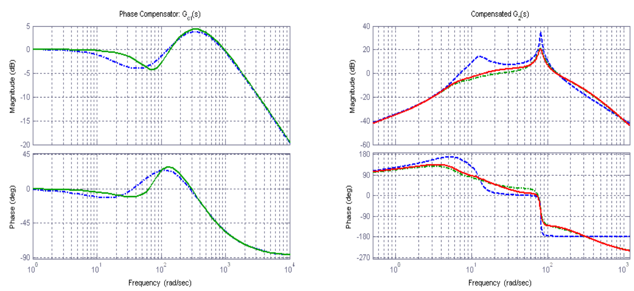

Fig. 8. Phase compensator $G_{c1}(s)$ (left), compensated $G_2(s)$ (right): lag/notch (solid), triple lead/lag (dash-dot), uncompensated (dash)

As shown in Fig. 8, both compensators (Eqs. 8,9 and 10) enhanced the feedback system's robustness by introducing gain margin of 14.5 dB and phase margin of 45°.

D. Human-in-the-Loop Experimental Results Using HIL Setup

Due to space limitation, only experimental results of the closed loop system with the triple lead/lag compensator (Eqs. 8, 9) are presented in the following. The experimental conditions are: $v_x = 120km/h$, $\mu = 0.8$ and the steering wheel angle $\theta_2(t) = 20^\circ sin(\pi t)$. Shown in Fig. 10 are the plots of: the steering wheel angle, the torsion bar, the assist-motor current and the Lissajous curve between the steering wheel angle and the torsion bar.

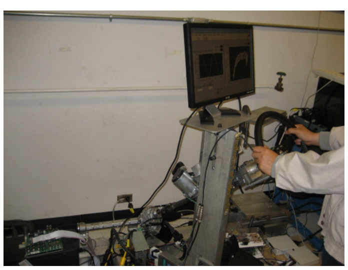

Fig. 9. Hardware-in-the-loop (HIL) experimental setup

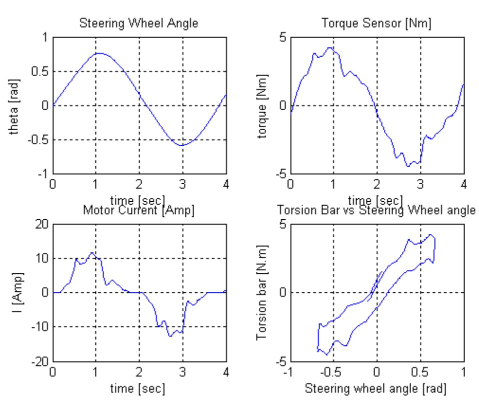

Fig. 10. Measurements of the closed loop system

The effect of road-tire disturbance is investigated using $f_{dist}(t) = 200sin(2\pi 12t)$ [N] at $v_x = 80km/h$ which is equivalent to tire-imbalance at 12 Hz. As shown by the Lissajous curve in Fig. 11, the 2-DOF controller structure has significantly reduced the effect of the disturbance on the steering "feel" in comparison to the feedback system with the phase compensator (Eq. 9) only.

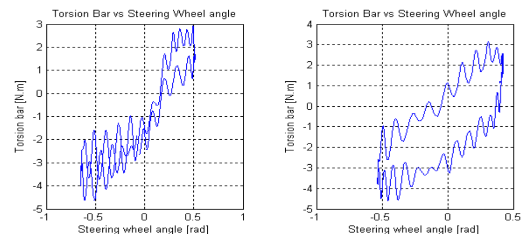

Fig. 11. Effect of disturbance on Lissajous cruve: phase compensator (left), 2-DOF compensator (right)

VI. Conclusions

This paper presented a 2-DOF fixed-structure controller for EPS systems. The controller is synthesized using hybrid GA/LMI optimization. The experimental results obtained show that the controller did satisfy the performance objectives defined in section 3. Specifically, absence of oscillations in the Lissajous curve and reduced phase lag between the steering angle and the input steering torque indicate "good" steering "feel" [9].

VII. Acknowledgments

The authors gratefully acknowledge the National Instruments and NSK (Japan) for their generous hadrware/software support. Finally, the authors would like to acknowledge the valuable comments provided by the anonymous reviewers.

References

[1] N. Bajcinca, et. al. Robust Control for Steer-by-Wire Vehicles. *Autonomous Robots*, vol. 19, 2005.

[2] J. Bernussou, et. al. On Strict Positive Real Systems Design. *Systems and Control Letters*, 36, 1999.

[3] A. Bootz, et. al. Efficiency Analysis of Hydraulic Power Steering Systems. *8th Scandinavian Conference on Fluid Power*, Finland, 2003.

[4] S. P. Boyd, et. al. *Linear Matrix Inequalities in System and Control Theory*. Society of Industrial and Applied Mathematics, 1994.

[5] C. Canudas-De-Wit, et. al. Fun-to-Drive by Feedback. *European Journal of Control*, 11(4/5), 2005.

[6] R. C. Chabaan and L. L. Wang. H_∞ Control of Electrical Power Assist Systems. *5th Int'l Symposium on Advanced Vehicle Control*, Michigan, 2000.

[7] J. E. Colgate. Robust Impedance Shaping Telemanipulation. *IEEE Transactions on Robotics and Automation*, 9(4), 1993.

[8] C. A. Desoer and M. Vidyasagar. *Feedback Systems: Input-Output Properties*. Academic Press, 1975.

[9] A. H. El-Shaer. Robust Control Design of Electric Power Steering Systems. Dept. of Mech. Engr. UC Berkeley PhD thesis, 2008.

[10] H. Khalil. *Nonlinear Systems*. Prentice Hall, 1996.

[11] P. Li. Towrads Safe and Friendly Hydraulics: The passive Valve. *ASME Journal of Dynamic Systems, Measurement and Control*, 122, 2000.

[12] J. Lofberg. YALMIP. http://control.ee.ethz.ch/joloef/yalmip.php.

[13] Z. Michalewicz. *Genetic Algorithms + Data Structure = Evolution Programs*. Springer-Verlag 1996.

[14] A. J. Pick and D. J. Cole. Measurement of Driver Steering Torque Using Electromyography. *ASME Journal of Dynamic Systems, Measurement and Control*, 128, 2006.

[15] C. C. Sun and H. Y. Chung. H_2/H_∞ Robust Static Output Feedback Control Design Via Mixed Genetic Algorithm and LMIs. *ASME Journal of Dynamic Systems, Measurement and Control*, 127, 2005.

[16] A. Zaremba, et. al. Vibration Control based on Dynamic Compensation in an Electric Power Steering System. *Control and Decision Conference*, 1997.